

Electronic order induced symmetry breaking in lattice dynamics of $\text{Co}_3\text{Sn}_2\text{S}_2$

Shuai Zhang,¹ Mengqi Wang,¹ and Tiantian Zhang^{1,*}

¹*Institute of Theoretical Physics, Chinese Academy of Sciences, Beijing 100190, China*

Based on the molecular Berry curvature (MBC) framework, we develop an *ab initio* algorithm to capture the quantitative effects of magnetic order on lattice dynamics. Using the ferromagnetic Weyl semimetal $\text{Co}_3\text{Sn}_2\text{S}_2$ as a prototype, we show that electronic-order-driven phonon symmetry breaking requires spin-orbit coupling (SOC) and leads to an MBC term that breaks both time-reversal (\mathcal{T}) and mirror symmetries. We demonstrate that mirror-symmetry breaking is essential to account for the experimentally observed phonon splitting, \mathcal{T} -breaking alone is insufficient. The MBC is widely distributed across the Brillouin zone, giving rise to significant off- Γ effects. Our results show the phonon splitting of the E_g and E_u modes have distinct origins: the E_g splitting arises from MBC and is captured by our algorithm, while the E_u splitting stems from correlation-sensitive Fano resonance, explaining their asymmetric experimental line shapes. We provide a design strategy and computational pathway for materials with large phonon magnetism and splitting, requiring SOC, electron-phonon coupling, and ideally flat bands at the Fermi level. This work also suggests new avenues for controlling non-reciprocal phonon transport.

Within Landau's theory, electronic orders, such as magnetic/spin, charge, and orbital order, are typically characterized by local order parameters and strong electron interactions, and are invariably accompanied by spontaneous symmetry breaking. This contrasts with phonon systems, where such symmetry breaking is rare. Recent work has shown that time-reversal symmetry (\mathcal{T}) breaking occurs in phonons by coupling to external fields [1–4], spins [5, 6] and chiral excitations [7]. Moreover, phonon energy splitting in ferromagnetic (FM) Weyl semimetal $\text{Co}_3\text{Sn}_2\text{S}_2$ directly demonstrates this effect [8, 9]. Although *ab initio* methods can readily describe electronic symmetry breaking, such as \mathcal{T} in magnetic systems, the concomitant symmetry breaking in the phonon system induced by electronic order remains inadequately explored by first-principles calculations. Thus, a quantitative understanding of symmetry breaking in lattice dynamics from first principles [10–12] is essential, and it is crucial for interpreting phonon-related transport [4, 13–20] and optical properties [1, 8, 9, 21, 22].

To capture the experimentally observed phonon splitting in $\text{Co}_3\text{Sn}_2\text{S}_2$, which is induced by magnetic order, we develop an *ab initio* algorithm based on molecular Berry curvature (MBC, or nuclear Berry curvature) theory. A nonzero MBC contribution necessitates the inclusion of spin-orbit coupling (SOC) [10]. This requirement distinguishes our approach from the phonon self-energy method in Ref. [11], which yields phonon splitting even in the absence of SOC. Under FM order and SOC, the MBC contribution breaks both \mathcal{T} and mirror symmetries in $\text{Co}_3\text{Sn}_2\text{S}_2$. Our results demonstrate that this mirror-symmetry breaking is essential to explain the observed phonon splitting in $\text{Co}_3\text{Sn}_2\text{S}_2$, as \mathcal{T} breaking alone is insufficient [23]. Furthermore, there's a broad Brillouin zone (BZ) distribution of the MBC contributions, leading to significant effects away from the Γ -point. Both mirror-symmetry breaking and off- Γ effects, which remain largely unexplored, are critical for a complete theoretical description of the lattice dynamics in $\text{Co}_3\text{Sn}_2\text{S}_2$. Furthermore, our results demonstrate

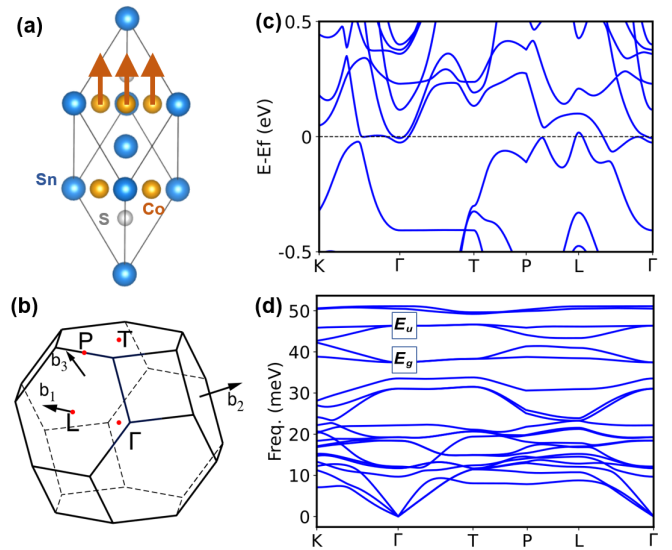


FIG. 1. The crystal structure, Brillouin zone, electronic/phonon structure of $\text{Co}_3\text{Sn}_2\text{S}_2$. (a) Crystal structure of $\text{Co}_3\text{Sn}_2\text{S}_2$. Brown arrows indicate the local magnetic moments on Co atoms. This magnetic order breaks the vertical mirror and time-reversal symmetry, but keeps the C_3 and inversion symmetry. (b) Brillouin zone of $\text{Co}_3\text{Sn}_2\text{S}_2$. (c) Electronic band structure with FM order and spin-orbit coupling. (d) Phonon spectrum of $\text{Co}_3\text{Sn}_2\text{S}_2$ without the molecular Berry curvature contribution. The coordinates of K are $(\frac{1}{3}, 0, -\frac{1}{3}) / (\frac{1}{3}, \frac{1}{3}, 0)$ in the basis of the primitive/conventional lattice vectors.

that the magnitude of the phonon splitting, while relevant for circularly polarized phonons with nonzero angular momentum (i.e., chiral phonons), is not uniquely determined by its absolute value.

Lattice dynamics for $\text{Co}_3\text{Sn}_2\text{S}_2$ without MBC $\text{Co}_3\text{Sn}_2\text{S}_2$ is the first experimentally confirmed magnetic Weyl semimetal [24–33] with a centrosymmetric space group of $R\bar{3}m$ (\mathcal{P} -preserving), thus the phonon modes can be classified in Raman active ones and infrared (IR) active ones at Γ . Figure 1(a) shows the primitive cell of $\text{Co}_3\text{Sn}_2\text{S}_2$ with brown arrows indicating the local magnetic moment. Below

* tzhang@itp.ac.cn

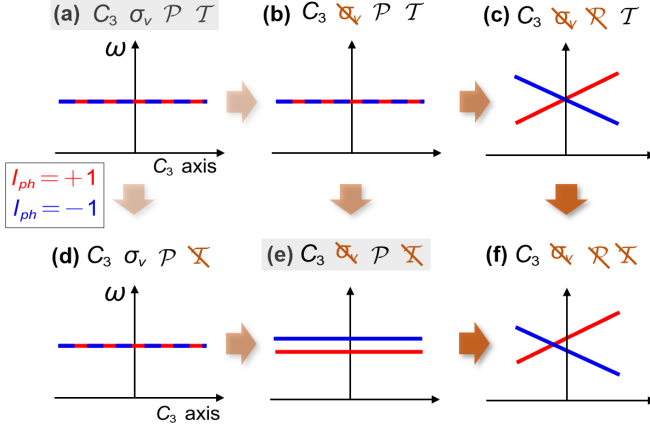


FIG. 2. Phonon spectra near the Γ point under successive symmetry-breaking conditions. From (a) to (c), vertical mirror symmetry (σ_v) and inversion symmetry (\mathcal{P}) are progressively broken. From top to bottom, time-reversal symmetry (\mathcal{T}) is broken. Since $\text{Co}_3\text{Sn}_2\text{S}_2$ belongs to the D_{3d} point group, breaking \mathcal{T} alone is insufficient to lift the phonon degeneracy, as seen between (a) and (d). Therefore, the MBC mechanism, which involves spin-orbit coupling and breaks σ_v , is necessary to split the degenerate modes.

$T_C \sim 175$ K [27–29, 34–38], FM order with C_3 axis spin alignment breaks both \mathcal{T} and vertical mirror symmetry, enabling an SOC-essential Weyl semimetal phase, reducing the point group from D_{3d} to C_{3i} (magnetic space group $R\bar{3}m'$).

Figure 1(c) presents the electronic band structure of $\text{Co}_3\text{Sn}_2\text{S}_2$ with FM order and SOC. The Fermi level has been shifted by 25 meV to align with the in-plane flat band position observed by the scanning tunneling microscopy [39]. The electronic bands near the Fermi level are primarily contributed by the d -orbitals of Co atoms.

Figure 1(d) displays the phonon spectrum without the MBC contribution. The highlighted E_u and E_g modes correspond to those observed experimentally [8, 9], and will be discussed in detail through quantitative comparisons. The sole E_g mode arises from S atoms occupying the $6c$ Wyckoff positions, which lacks inversion site-symmetry. In contrast, Co, Sn_1 and Sn_2 reside at the Wyckoff positions of $9e$, $3a$ and $3b$, respectively, all of them preserve inversion site-symmetry. The atomic displacements transform as a vector representation under $O(3)$ operations, analogous to p -orbitals, and exhibit odd parity. As a result, neither Co nor Sn can generate phonon modes of even parity.

The degeneracy of the E_g and E_u modes along the C_3 -invariant path, i.e., $-\Gamma \leftrightarrow \Gamma \leftrightarrow \Gamma$, is protected by vertical mirror symmetry as well as \mathcal{PT} symmetry [23]. The experimental observation of phonon splitting thus implies the breaking of both \mathcal{PT} and vertical mirror symmetry, as shown in Fig. 2(e). To quantitatively describe the underlying physical mechanism, we develop a *ab initio*+MBC algorithm based on the Wannier basis to efficiently quantify this ferromagnetism-induced $E_{g/u}$ splitting.

MBC modified lattice dynamics Experiments rule out resonant magnon-phonon coupling in $\text{Co}_3\text{Sn}_2\text{S}_2$ [40], allowing it

to be safely discounted for an accurate description of the lattice dynamics [2, 10]. Furthermore, Ref. [9] confirms weak electron-hole pair excitation in $\text{Co}_3\text{Sn}_2\text{S}_2$, preserving Born-Oppenheimer approximation (BOA) validity for MBC calculations. Within the BOA, the adiabatic evolution of the electronic ground state with the lattice accumulates a Berry phase, which subsequently couples back to influence lattice dynamics [20, 41], thus the equation of motion (EOM) reads:

$$[\tilde{K}(\mathbf{q}) + \tilde{G}^\dagger(\mathbf{q})\tilde{G}(\mathbf{q})]\epsilon_{\nu\mathbf{q}} = \omega_{\nu\mathbf{q}}^2 \epsilon_{\nu\mathbf{q}} - 2i\omega_{\nu\mathbf{q}}\tilde{G}(\mathbf{q})\epsilon_{\nu\mathbf{q}}, \quad (1)$$

where $\epsilon_{\nu\mathbf{q}}$ is the polarization vector, $\tilde{K}_{\kappa\alpha,\kappa'\beta}(\mathbf{q}) = \frac{1}{\sqrt{M_\kappa M_{\kappa'}}} K_{\kappa\alpha,\kappa'\beta}(\mathbf{q})$ and $\tilde{G}_{\kappa\alpha,\kappa'\beta}(\mathbf{q}) = \frac{1}{2\sqrt{M_\kappa M_{\kappa'}}} G_{\kappa\alpha,\kappa'\beta}(\mathbf{q})$ are the mass-weighted dynamic matrix and MBC. To solve this equation, we can take $\tilde{G}(\mathbf{q})$ as the first-order perturbation, and discard the second-order perturbation $\tilde{G}^\dagger(\mathbf{q})\tilde{G}(\mathbf{q})$. The zero-order equation reads:

$$\tilde{K}(\mathbf{q})\epsilon_{\nu\mathbf{q}}^{(0)} = \omega_{\nu\mathbf{q}}^{(0)2} \epsilon_{\nu\mathbf{q}}^{(0)}, \quad (2)$$

and the first-order modification of $\omega_{\nu\mathbf{q}}^{(0)2}$ reads

$$\Delta\omega_{\nu\mathbf{q}}^{(0)2} = \langle \epsilon_{\nu\mathbf{q}} | 2i\omega_{\nu\mathbf{q}}^{(0)} \tilde{G}_{\kappa\alpha,\kappa'\beta}(\mathbf{q}) | \epsilon_{\nu'\mathbf{q}} \rangle. \quad (3)$$

$\nu = \nu'$ for the non-degenerated case. Detailed discussions are in the Supplementary Material.

Standard first-principles calculations of the dynamical matrix K_{ij} preserve the symmetries that are broken by the electronic FM order parameterized via a pseudovector, such as \mathcal{T} and vertical mirror symmetry (see Supplementary Material). Thus, this algorithmic limitation results in a spurious double degeneracy of the E_g and E_u phonon modes, as shown in Fig. 2(a). Although the MBC term \tilde{G} was proposed to break \mathcal{T} -symmetry [10, 20], it alone is insufficient to lift the degeneracy of phonon bands along the C_{3v} -invariant high-symmetry path ($-\Gamma \leftrightarrow \Gamma \leftrightarrow \Gamma$) in $\text{Co}_3\text{Sn}_2\text{S}_2$, due to the presence of vertical mirror symmetry [23], as illustrated in Fig. 2(d). Therefore, an additional mechanism breaking the both of the \mathcal{T} and vertical mirror symmetry by MBC is essential to explain the experimentally observed phonon splitting in Fig. 2(e).

MBC-modified E_g mode Figure 3(a) displays the phonon spectra of the E_g mode with MBC along the C_3 -invariant path $-\Gamma \leftrightarrow \Gamma \leftrightarrow \Gamma$. Within our *ab initio* framework, MBC lifts the degeneracy along the entire path by breaking both time-reversal \mathcal{T} (as well as \mathcal{PT}) and vertical mirror symmetries. The magnitude of the phonon energy splitting for the E_g modes is presented in Fig. 3(b), revealing a maximum splitting at the Γ point and a minimum splitting at T.

At Γ , the calculated phonon splitting is approximately 0.253 meV (2.05 cm^{-1}), which agrees with the experimental value of 1.27 cm^{-1} reported in Ref. [8] in order of magnitude. The minor discrepancy may originate from slight variations in the experimental Fermi level and anharmonic effects [42, 43]. To further investigate the influence of the Fermi level on the MBC, we shifted it by 60 meV and recalculated the splitting of the E_g mode. This adjustment yields a splitting of approximately 1.24 cm^{-1} , which is in excellent agreement with the experimental value (see Supplementary Material for details).

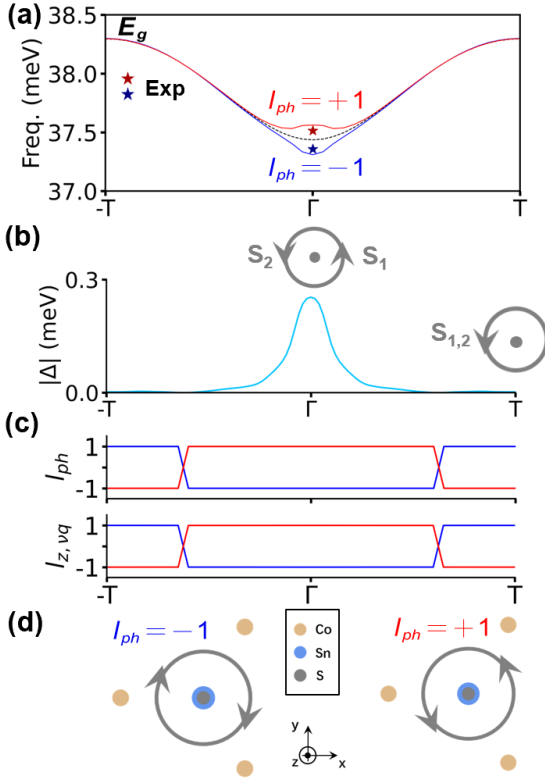


FIG. 3. The MBC induced splitting for E_g mode. (a) Phonon dispersion of the E_g mode along the C_3 -invariant path $-\Gamma \leftrightarrow \Gamma \leftrightarrow \Gamma$, calculated without (black dashed line) and with molecular Berry curvature (blue and red solid lines). The colored stars mark the energy positions of the E_g mode observed experimentally. (b) Energy splitting of the E_g mode along the C_3 -invariant path. The insert figure shows the vibrational modes of the S atoms at the Γ and T points. (c) Evolution of the pseudo-angular momentum (l_{ph}) and the z-component of the angular momentum ($l_{z,vq}$) along the C_3 -invariant path. (d) Atomic displacement patterns of the two E_g modes at the Γ point.

To further elucidate the lattice dynamics of E_g induced by MBC, we calculate both the pseudo-angular momentum (l_{ph}) and the z-component of the angular momentum ($l_{z,vq}$) along the C_3 -invariant path, as shown in Fig. 3(c). We note the angular momentum only has z component due to the restriction of C_3 symmetry [23]. Both quantities exhibit a quantized value of unity, with sign reversals resulting from band inversion along the path, which fundamentally governs the emergence of the phonon Hall effect [4, 13–20].

The quantized unity of the l_{ph} arises from the C_3 symmetry of the system. In contrast, the quantization of $l_{z,vq}$ along the path $-\Gamma \leftrightarrow \Gamma \leftrightarrow \Gamma$ can be attributed to two factors: (i) At Γ , E_g is contributed solely by the vibration of S atoms residing at C_3 -invariant Wyckoff positions [23, 44]. As illustrated in Fig. 3(d), these two S atoms rotate in the same direction but with a π phase difference at the Γ . (ii) Away from Γ , their energies are well-separated from other modes, resulting in minimal hybridization with other phonon modes.

It should be noted that the phonon splitting induced by MBC is not uniquely determined by $l_{z,vq}$. As shown in

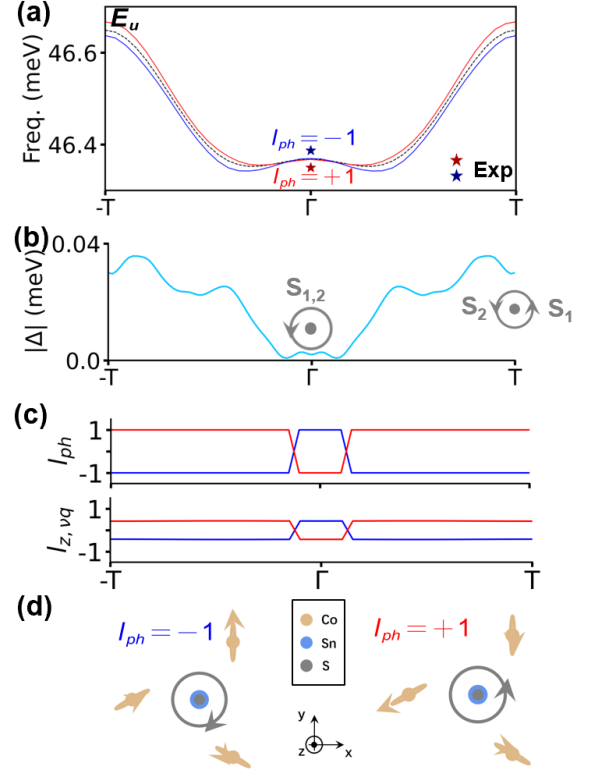


FIG. 4. The MBC induced splitting for E_u mode. (a) Phonon dispersion of the E_u mode along the C_3 -invariant path $-\Gamma \leftrightarrow \Gamma \leftrightarrow \Gamma$, calculated without (black dashed line) and with molecular Berry curvature (blue and red solid lines). The colored stars mark the energy positions of the E_u mode observed experimentally. (b) Energy splitting of the E_u mode along the C_3 -invariant path. The insert figure shows the vibrational modes of the S atoms at the Γ and T points. (c) Evolution of the pseudo-angular momentum (l_{ph}) and the z-component of the angular momentum ($l_{z,vq}$) along the C_3 -invariant path. (d) Atomic displacement pattern of the two E_u modes at the Γ point.

Figs. 3(b) and (c), $l_{z,vq}$ remains close to unity along the C_3 -invariant path, yet the splitting of the E_g modes varies significantly with a maximum at Γ .

MBC-modified E_u mode Figure 4(a) displays the MBC-modified phonon spectra of the E_u mode along the path $-\Gamma \leftrightarrow \Gamma \leftrightarrow \Gamma$. The MBC also lifts the degeneracy of the E_u mode (dashed line) across the entire $-\Gamma \leftrightarrow \Gamma \leftrightarrow \Gamma$ path. The magnitude of the phonon energy splitting for the Eg modes is presented in Fig. 4(b), revealing a maximum splitting in the vicinity of T and minimum splitting in the vicinity of Γ .

Combined with Figs. 3(b) and 4(b), it can be observed that although the parity of the E_g and E_u modes remains unchanged at both Γ and T, the relative phase between the two S atoms shifts by π . For instance, the E_g mode exhibits a relative phase of π at Γ but 0 at T, whereas the E_u mode shows a phase of 0 at Γ and π at T. This switching of the relative phase between the two modes correlates with the reversal of the maximum phonon splitting.

At the Γ point, the splitting calculated from our algorithm is about 0.002 meV (0.016 cm^{-1}), which is smaller than the

experimentally observed value of 0.3 cm^{-1} reported in the optical conductivity measurements [9]. This discrepancy suggests that the splitting observed in experiments is not primarily caused by the MBC. Combined with the asymmetric line shapes of the E_u mode, we attribute the larger experimental splitting to a Fano resonance [9]. This resonance may arise from quantum interference between electronic and phonon excitations when Weyl cones approach the Fermi level [45, 46]. The absence of an asymmetric line shape in the E_g mode further supports this interpretation, indicating that the phonon splitting mechanisms for the E_g and E_u modes are distinct.

We note that the energy splitting of the E_u mode is significantly smaller than that of the E_g mode at Γ point, a result captured by both our *ab initio* calculations and experimental measurements [8, 9]. Moreover, We notice both the E_g and E_u modes exhibit a broad distribution of splitting across the entire BZ, rather than being concentrated solely at the high-symmetry momentum. This widely distributed chiral phonon dynamics may give rise to observable transport signatures associated with phonon chirality.

Fig. 4(c) displays the distributions of pseudo-angular momentum and angular momentum for the two split E_u modes. The angular momentum of these modes is not quantized to unity, which can be attributed to the vibration from both Co and S atoms. As illustrated in Fig. 4(d), the Co atoms are not located at C_3 -invariant Wyckoff positions, thus resulting in a non-quantized values of angular momentum [23].

Phonon splitting and magnetism under MBC To explain the distinct magnitude of the energy splitting for the E_g and E_u modes at the Γ point, we calculate the distribution of the mode-resolved MBC, denoted as $\tilde{G}(\Gamma, \mathbf{k}, \mathbf{k})$, across the electronic BZ, as shown in Fig. 5. The results indicate that $\tilde{G}_{E_u}(\Gamma, \mathbf{k}, \mathbf{k})$ is significantly smaller in magnitude than $\tilde{G}_{E_g}(\Gamma, \mathbf{k}, \mathbf{k})$, consistent with our earlier findings on MBC-induced phonon splitting. Furthermore, we observe that the distribution of $\tilde{G}_{E_u}(\Gamma, \mathbf{k}, \mathbf{k})$ exhibits substantial cancellation between positive and negative contributions. This cancellation further explains the markedly smaller MBC-induced splitting of the E_u mode compared to the E_g mode.

Previous studies have attributed Γ -point phonon splitting under external magnetic fields to the manifestation of an effective phonon magnetic moment (M_z) [1–4]. As detailed in Ref. [3], M_z comprises two contributions: one from the Born effective charges and another from the Berry curvature of electrons in both real space (MBC) and momentum space (Ω_e), i.e.,

$$M_z = \frac{e}{2M_K} l_{z,yq} \int d\mathbf{k} \left\{ \Omega_{k_x u_y} - \Omega_{k_y u_x} + \Omega_{e,k_x k_y} G_{u_x u_y} \right\}. \quad (4)$$

The first two terms collectively integrate to the Born effective charge, whereas the third term is equivalent to the product of the conventional electronic and molecular Berry curvatures. In $\text{Co}_3\text{Sn}_2\text{S}_2$, the metallic nature and the preservation of \mathcal{P} result in a vanishing Born effective charge. Given that G is independent of \mathbf{k} and the integral $\int d\mathbf{k} \Omega_{e,k_x k_y}$ is proportional to the anomalous Hall conductivity σ_{xy}^A , the expression for the phonon magnetic moment simplifies to $M_z \propto l_{z,yq} \cdot G \cdot \sigma_{xy}^A$. Consequently, the large intrinsic Hall conductivity

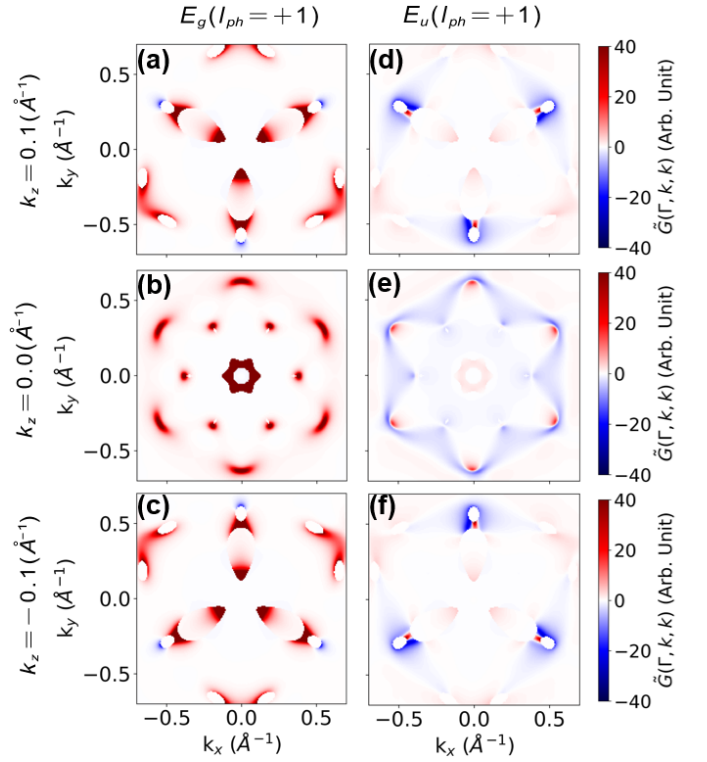


FIG. 5. Distribution of the MBC in the electronic BZ. (a-c) are MBC distributions for the E_g phonon mode with $l_{ph} = +1$ on three distinct k_z planes. The MBC distribution for the E_g mode with $l_{ph} = -1$ is of opposite sign. (d-f) are MBC distributions for the E_u mode with $l_{ph} = +1$. The E_u mode with $l_{ph} = -1$ also exhibits a sign reversal. The MBC magnitude is significantly larger for the E_g modes than for the E_u modes, which consequently results in a smaller calculated phonon splitting for the E_u modes.

ity of $\text{Co}_3\text{Sn}_2\text{S}_2$ (approximately $505 \Omega^{-1} \text{ cm}^{-1}$ [25]) indicates a strong propensity for intrinsic phonon magnetism in this material. As calculated and shown in Fig. 5, the pronounced difference in the MBC between the E_g and E_u modes indicates a larger magnetic moment for the E_g phonon.

In summary, our *ab initio*-MBC methodology captures the electronic order-induced symmetry breaking in the lattice dynamics of $\text{Co}_3\text{Sn}_2\text{S}_2$, generalizing the manifestation of phonon magnetism and phonon energy shift effects in magnetic materials. Notably, the energy scale of circularly polarized phonons coincides with that of chiral Weyl fermions, suggesting rich opportunities for chiral boson–fermion coupling and enabling control over topological states through phononic and magnetic means [47]. This efficient and accurate framework for magnetic lattice dynamics is readily extendable to full Brillouin-zone calculations and enables the study of emergent phenomena such as the phonon Hall effect [4, 13–20], Hall viscosity [48], and so on. The algorithm is broadly applicable to intrinsic magnetic systems, facilitating the discovery of materials with large phonon magnetism.

Our findings establish a set of design principles for materials with large phonon magnetic moments and substantial splitting, i.e., strong spin-orbit coupling, significant electron-

- [28] N. Morali, R. Batabyal, P. K. Nag, E. Liu, Q. Xu, Y. Sun, B. Yan, C. Felser, N. Avraham, and H. Beidenkopf, Fermi-arc diversity on surface terminations of the magnetic weyl semimetal $\text{Co}_3\text{Sn}_2\text{S}_2$, *Science* **365**, 1286 (2019).
- [29] W. Yan, X. Zhang, Q. Shi, X. Yu, Z. Zhang, Q. Wang, S. Li, and H. Lei, Critical behavior of half-metallic ferromagnet $\text{Co}_3\text{Sn}_2\text{S}_2$, *Solid State Communications* **281**, 57 (2018).
- [30] R. Yang, T. Zhang, L. Zhou, Y. Dai, Z. Liao, H. Weng, and X. Qiu, Magnetization-induced band shift in ferromagnetic weyl semimetal $\text{Co}_3\text{Sn}_2\text{S}_2$, *Phys. Rev. Lett.* **124**, 077403 (2020).
- [31] Z. Y. Liu, T. Zhang, S. X. Xu, P. T. Yang, Q. Wang, H. C. Lei, Y. Sui, Y. Uwatoko, B. S. Wang, H. M. Weng, J. P. Sun, and J.-G. Cheng, Pressure effect on the anomalous hall effect of ferromagnetic weyl semimetal $\text{Co}_3\text{Sn}_2\text{S}_2$, *Phys. Rev. Mater.* **4**, 044203 (2020).
- [32] Y. Xu, J. Zhao, C. Yi, Q. Wang, Q. Yin, Y. Wang, X. Hu, L. Wang, E. Liu, G. Xu, L. Lu, A. A. Soluyanov, H. Lei, Y. Shi, J. Luo, and Z.-G. Chen, Electronic correlations and flattened band in magnetic weyl semimetal candidate $\text{Co}_3\text{Sn}_2\text{S}_2$, *Nature Communications* **11**, 3985 (2020).
- [33] M. Kanagaraj, J. Ning, and L. He, Topological $\text{Co}_3\text{Sn}_2\text{S}_2$ magnetic weyl semimetal: From fundamental understanding to diverse fields of study, *Reviews in Physics* **8**, 100072 (2022).
- [34] E. Liu, Y. Sun, N. Kumar, L. Muechler, A. Sun, L. Jiao, S.-Y. Yang, D. Liu, A. Liang, Q. Xu, J. Kroder, V. Süß, H. Borrmann, C. Shekhar, Z. Wang, C. Xi, W. Wang, W. Schnelle, S. Wirth, Y. Chen, S. T. B. Goennenwein, and C. Felser, Giant anomalous hall effect in a ferromagnetic kagome-lattice semimetal, *Nature Physics* **14**, 1125 (2018).
- [35] Q. Wang, Y. Xu, R. Lou, Z. Liu, M. Li, Y. Huang, D. Shen, H. Weng, S. Wang, and H. Lei, Large intrinsic anomalous hall effect in half-metallic ferromagnet $\text{Co}_3\text{Sn}_2\text{S}_2$ with magnetic weyl fermions, *Nature Communications* **9**, 3681 (2018).
- [36] R. Wehrich, I. Anusca, and M. Zabel, Half-antiperovskites: Structure and type-antitype relations of shandites $m_3/2a_8$ (m : Co, ni; a : In, sn), *ChemInform* **36**, no (2005).
- [37] P. Vaqueiro and G. G. Sobany, A powder neutron diffraction study of the metallic ferromagnet $\text{Co}_3\text{Sn}_2\text{S}_2$, *Solid State Sciences* **11**, 513 (2009).
- [38] W. Schnelle, A. Leithe-Jasper, H. Rosner, F. M. Schappacher, R. Pöttgen, F. Pielhofer, and R. Wehrich, Ferromagnetic ordering and half-metallic state of $\text{Sn}_2\text{Co}_3\text{S}_2$ with the shandite-type structure, *Phys. Rev. B* **88**, 144404 (2013).
- [39] J.-X. Yin, S. S. Zhang, G. Chang, Q. Wang, S. S. Tsirkin, Z. Guguchia, B. Lian, H. Zhou, K. Jiang, I. Belopolski, N. Shumiya, D. Multer, M. Litskevich, T. A. Cochran, H. Lin, Z. Wang, T. Neupert, S. Jia, H. Lei, and M. Z. Hasan, Negative flat band magnetism in a spin-orbit-coupled correlated kagome magnet, *Nature Physics* **15**, 443 (2019).
- [40] C. Liu, J. Shen, J. Gao, C. Yi, D. Liu, T. Xie, L. Yang, S. Danilkin, G. Deng, W. Wang, S. Li, Y. Shi, H. Weng, E. Liu, and H. Luo, Spin excitations and spin wave gap in the ferromagnetic weyl semimetal $\text{Co}_3\text{Sn}_2\text{S}_2$, *Science China Physics, Mechanics & Astronomy* **64**, 217062 (2021).
- [41] T. Qin, Q. Niu, and J. Shi, Energy magnetization and the thermal hall effect, *Phys. Rev. Lett.* **107**, 236601 (2011).
- [42] B. Wei, Q. Sun, C. Li, and J. Hong, Phonon anharmonicity: a pertinent review of recent progress and perspective, *Science China Physics, Mechanics & Astronomy* **64**, 117001 (2021).
- [43] Q.-Y. Xie, F. Xiao, K.-W. Zhang, and B.-T. Wang, Anharmonic phonon self-energy and anomalous thermal transport in the quaternary compound $\text{BaAg}_2\text{SnSe}_4$, *Phys. Rev. B* **110**, 045203 (2024).
- [44] T. Zhang and S. Murakami, Chiral phonons and pseudoangular momentum in nonsymmorphic systems, *Physical Review Research* **4**, L012024 (2022).
- [45] M. J. Rice, Organic linear conductors as systems for the study of electron-phonon interactions in the organic solid state, *Phys. Rev. Lett.* **37**, 36 (1976).
- [46] E. Cappelluti, L. Benfatto, M. Manzardo, and A. B. Kuzmenko, Charged-phonon theory and Fano effect in the optical spectroscopy of bilayer graphene, *Physical Review B* **86**, 115439 (2012).
- [47] F. G. Hernandez, A. Baydin, S. Chaudhary, F. Tay, I. Katayama, J. Takeda, H. Nojiri, A. K. Okazaki, P. H. Rappl, E. Abramof, et al., Observation of interplay between phonon chirality and electronic band topology, *Science advances* **9**, eadj4074 (2023).
- [48] S. Heidari, A. Cortijo, and R. Asgari, Hall viscosity for optical phonons, *Phys. Rev. B* **100**, 165427 (2019).
- [49] T. Nomura, X.-X. Zhang, R. Takagi, K. Karube, A. Kikkawa, Y. Taguchi, Y. Tokura, S. Zherlitsyn, Y. Kohama, and S. Seki, Nonreciprocal phonon propagation in a metallic chiral magnet, *Physical Review Letters* **130**, 176301 (2023).
- [50] Y. Ren, D. Saparov, and Q. Niu, Nonreciprocal phonons in pt -symmetric antiferromagnets, *Physical Review Letters* **134**, 206701 (2025).
- [51] R. Aoki, Y. Kousaka, and Y. Togawa, Anomalous nonreciprocal electrical transport on chiral magnetic order, *Physical Review Letters* **122**, 057206 (2019).